This is the accepted manuscript made available via CHORUS. The article has been published as:

Charge trapping at math xmlns="http://www.w3.org/1998/Math/MathML">mrow>mi >Al/mi>mo>//mo>msub>mi>Al/mi>mn>2/mn>/msub>/m row>msub>mrow>mi mathvariant="normal">O /mi>/mrow>mn>3/mn>/msub>/math> interface facilitates hydrogen-induced superabundant metal vacancy formation

Vrindaa Somjit and Bilge Yildiz

Phys. Rev. Materials **7**, L072001 — Published 25 July 2023

DOI: 10.1103/PhysRevMaterials.7.L072001

Charge trapping at $Al|Al_2O_3$ interface facilitates hydrogen-induced superabundant metal vacancy formation

Vrindaa Somjit[1] and Bilge Yildiz[2]

Abstract

Hydrogen is a ubiquitous impurity that deteriorates the metal|oxide interface, causing challenges such as current leakage and blistering. Here, we uncover the mechanisms behind hydrogen-induced damage at the prototypical $Al|Al_2O_3$ interface. The precursor that we identify is charge-trapping at the interface, which facilitates hydrogen segregation to the interface plane as H^-. Presence of hydrogen increases aluminum vacancy concentration at the interfacial metal and oxide planes. Each Al vacancy can trap multiple hydrogen atoms. As a result, the interfacial aluminum vacancy and hydrogen concentrations increase by orders-of-magnitude. Additionally, hydrogen behaves as an n-type dopant and increases electronic conductivity at the oxide layer adjacent to the interface by forming H^+, and the $[V_{Al}\text{-}H]$ complex is the predominant defect at this layer. These findings provide the precursor mechanisms of hydrogen-induced damage at the metal|oxide interfaces and have implications for advancing $Al|Al_2O_3$-based coatings and electronic devices.

Keywords

Hydrogen, ab initio, thermodynamics, superabundant vacancy, interface, corrosion, qubit, dielectric, interfacial electronic states.

[1] Department of Materials Science and Engineering, Massachusetts Institute of Technology, Cambridge, MA, USA
[2] Department of Nuclear Science and Engineering, Massachusetts Institute of Technology, Cambridge, MA, USA
Correspondence and Lead Contact: byildiz@mit.edu

The $Al|Al_2O_3$ interface is a canonical metal|oxide interface and is utilized in important applications, including protective coatings [1–4], micro-/nano-electronics [5–7], composites [1,8], catalyst supports [9], and hydrogen production [10]. The integrity of the interface and the electronic conductivity of the oxide play a critical role in the performance of these applications. Hydrogen, a ubiquitous impurity commonly found in most processing and operating environments, can incorporate into Al_2O_3 and Al, affecting these key properties. For example, hydrogen accumulation at the $Al|Al_2O_3$ interface is thought to cause blistering and spallation of the protective oxide, deteriorating protectiveness of the coating [11–14]. Hydrogen incorporation is known to increase the leakage current in $Al|Al_2O_3|Al$ tunnel junctions, leading to poor performance and device failure [15–17]. Hydrogen is also a two-level system in $Al|Al_2O_3$-based superconducting qubits, especially near surfaces and interfaces, leading to quantum decoherence [18–20].

Despite this pervasive effect of hydrogen on $Al|Al_2O_3$-based devices and coatings, atomic level understanding of the underlying mechanisms is still lacking. For example, it is unclear whether hydrogen-induced structural damage is initiated at the oxide side or the metal side of the interface. First principles studies propose interfacial blistering is mainly initiated by breaking of interfacial Al_{metal}-O bonds by hydrogen, and hydrogen accumulation in sub-interfacial cation vacancies in the oxide [12]. In contrast, experimental studies indicate that damage likely begins at the metal side, facilitated by interfacial weakening due to hydrogen and the resulting metal diffusion-induced interfacial cavitation [11]. The reason behind the increase in electronic conductivity upon hydrogen incorporation in Al_2O_3 films on Al is also unclear. First principles calculations suggest that non-bonded H interstitials [15] mediate electron tunneling through the oxide, whereas anodic polarization experiments indicate that the increase in conductivity is likely due to electron donation by the formation of positively charged defects [15,17] (such as H^+). Finally, in the context of two-level systems in $Al|Al_2O_3$ superconducting qubits, first principles calculations have only simulated hydrogen in bulk Al_2O_3, with different studies [19,20] attributing decoherence to different hydrogen defect species, such as H^+ interstitials [20] and $[V_{Al}\text{-}H]^q$ complexes (where q = charge state of complex) [19]. This highlights that explicit atomistic simulation of H defects at the interface between Al and Al_2O_3 would be desirable to reconcile these inconsistencies.

Here, we find that electronic charge trapped at the Al|Al_2O_3 interface causes hydrogen segregation to the interface. The segregation of hydrogen then reduces the formation energies of aluminum vacancies at the interfacial metal plane. This leads to the formation of superabundant vacancies, which in turn trap multiple hydrogen atoms. This self-catalytic mechanism is the likely precursor mechanism to cavitation and blistering at the interface. We also find that hydrogen forms H^+ at the oxide layer adjacent to the interface by donating its electron to the interfacial mid-gap states, which could explain the increase in conductivity of thin Al_2O_3 films. Lastly, we find that the [V_{Al}-H] complex is the predominant defect in this layer, which could be an important consideration for decoherence in superconducting qubits.

Details about the interface structure simulated [21], simulation technique (including parameters of our density functional theory (DFT) calculations) and defect formation energy calculations, are given in Supplementary Information Sections 1 and 2 [22] (see also references [23–43] therein). Specifically, the interface structure identified by *ab initio* Grand Canonical Monte Carlo (GCMC) under Al-rich, O-poor conditions (the conditions we expect at the equilibrated Al|Al_2O_3 interface from our previous work [21]) was used in this study. Al_2O_3 (0001) is strained in-plane to match the lattice parameters of Al (111), resulting in a misfit strain of ~3% (see Supplementary Information Section 1 for additional details [22]). The computed Al 2p and O 1s interfacial core level shifts of this interface closely match that of experiments, as discussed in [21], thereby making this a realistic interface structure to base our investigations upon. Defects investigated in this work include hydrogen bonded to interfacial under-coordinated Al (Al 'dangling bonds') from the oxide, hydrogen on FCC hollow sites at the interfacial metal layer, aluminum vacancies and aluminum vacancy-hydrogen complexes at the metal layer and oxide layer adjacent to the interface, and aluminum divacancies and their complexes with hydrogen at the interfacial metal layer. The relaxed structures of key defects studied are shown in **Figure 1**.

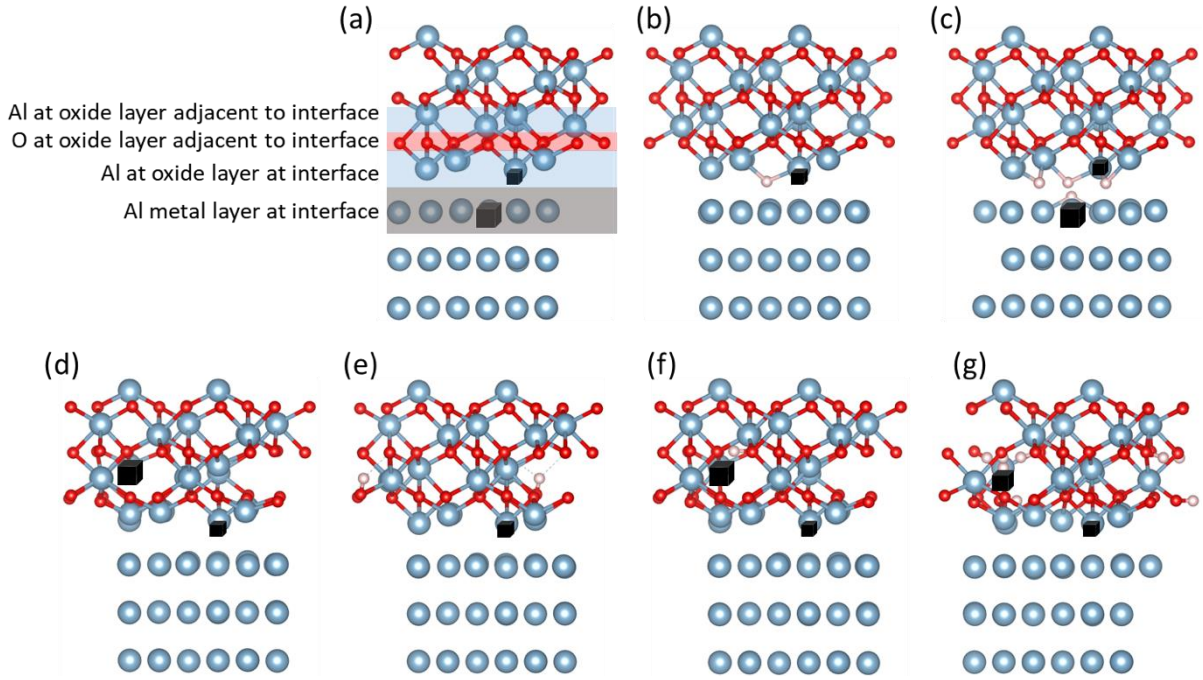


Figure 1. Relaxed structures of key defects at the interface ((a)-(c)) and at the oxide layer adjacent to the interface ((d)-(g)). Note that the oxide layer at the interface has 12.5% V_{Al} as found from ab initio GCMC calculations [21]. We depict this 'intrinsic' vacancy as a small black cube to differentiate it from the 'extrinsic' vacancies that we investigate in this study. We represent the latter as a large black cube. (a) V_{Al} (large black cube), (b) H_O, (c) [V_{Al}-4H] at the interfacial metal layer (d) V_{Al}, (e) H_{int}, (f) [V_{Al}-H], (g) [V_{Al}-5H] at the oxide layer adjacent to the interface. Only layers near the interface are shown. Red spheres- oxygen, blue spheres- aluminum, white spheres- hydrogen. (a) also denotes the nomenclature for the different regions at which defects were investigated.

Our first key observation is that hydrogen segregates to the interface with a segregation energy of 0.39 eV from the metal side and 3.2 eV from the oxide side ($E_{seg} = E_{f,H\ in\ metal\ or\ oxide} - E_{f,H\ at\ interface}$, where E_{seg} and E_f are the segregation and formation energies respectively, with $E_{f,H\ in\ metal\ or\ oxide}$ computed from separate simulations of H defects in bulk Al and bulk Al_2O_3; see Supplementary Section S2 for more details [22]). Note that the segregation energy from the oxide side is an order of magnitude higher than from the metal due to the high formation energy of H interstitial in the oxide compared to the metal. We tested several sites for hydrogen stability as detailed in Supplementary Information Section S3 [22]. Interestingly, H does not form H^+ and break interfacial Al-O bonds to bond with O at the interface. Instead, hydrogen is stable only either at the FCC hollow sites on the Al metal layer at the interface (H_{FCC}) or bonds with the under-

coordinated Al atoms at the oxide side of the interface, i.e., at the oxygen site (H_O). In both cases, H has a calculated Bader charge [44,45] of ~2, i.e., it exists as H^-.

This segregation of H to the interface can be understood by examining the electronic structure of the interface and the charge redistribution that occurs upon the addition of hydrogen at the interface. In our previous study on the Al|Al_2O_3 interface [21], Bader charge [44,45] analysis (**Figure 2**a) revealed that the interfacial Al atoms on the oxide side (labeled as layer Al4 in **Figure 2**c) on average each have one extra electron (compared to Al^{3+}) due to under-coordination. These excess electrons are accommodated in the mid-gap states made of Al 3s, 3p and O 2p from the oxide layer near the interface. This contribution of the interfacial Al atoms from the oxide side (Al4 layer in **Figure 2**c) to the mid-gap states can be seen in **Figure 2**b (top PDOS panel labeled 'Al4, no H', see also Figure 4 in Ref. [21]). In fact, this is reminiscent of an electride, where the electrons are spatially separated from the positively charged ions [46]. Upon introducing H at the interface, the H 1s orbital interacts strongly with these interfacial Al 3sp 'dangling bonds' to form H^- and therefore is trapped in stable Al-H bonds at the interface. This bond formation can be seen in the projected density of states plot in **Figure 2**b, where peaks made from the superposition of H and Al states (from interfacial Al4 layer) are seen deep in the valence band (at -9 to -11 eV). **Figure 2**c plots the charge density difference between the interface with H_O and the bare interface (i.e., $\rho_{interface\ with\ H_O} - \rho_{bare\ interface}$), showing the bond formation between under-coordinated interfacial cations and H. Crucially, this also explains why interfacial O-H bonds are not formed: H prefers to segregate to sites with high electron density to form H^- and a bonding state in the valence band, thus forming strong Al-H bonds, rather than form H^+ and weaken an existing Al-O bond to form a covalent O-H bond. Monte Carlo simulations with different H concentrations at different equilibrium interface structures found in our previous study [21] confirm this behavior (Supplementary Section S4 [22]). While we haven't explicitly quantified the effect of Al_2O_3 thickness on H-defect formation at the interface, the Monte Carlo simulations show that H segregation behavior is likely a very local effect, confined to the interfacial plane, and therefore is likely independent of the thickness or phase of the oxide layer. Note that similar H multicenter bond formation upon H substitution on an oxygen site has been reported in metal oxides like MgO and ZnO [47].

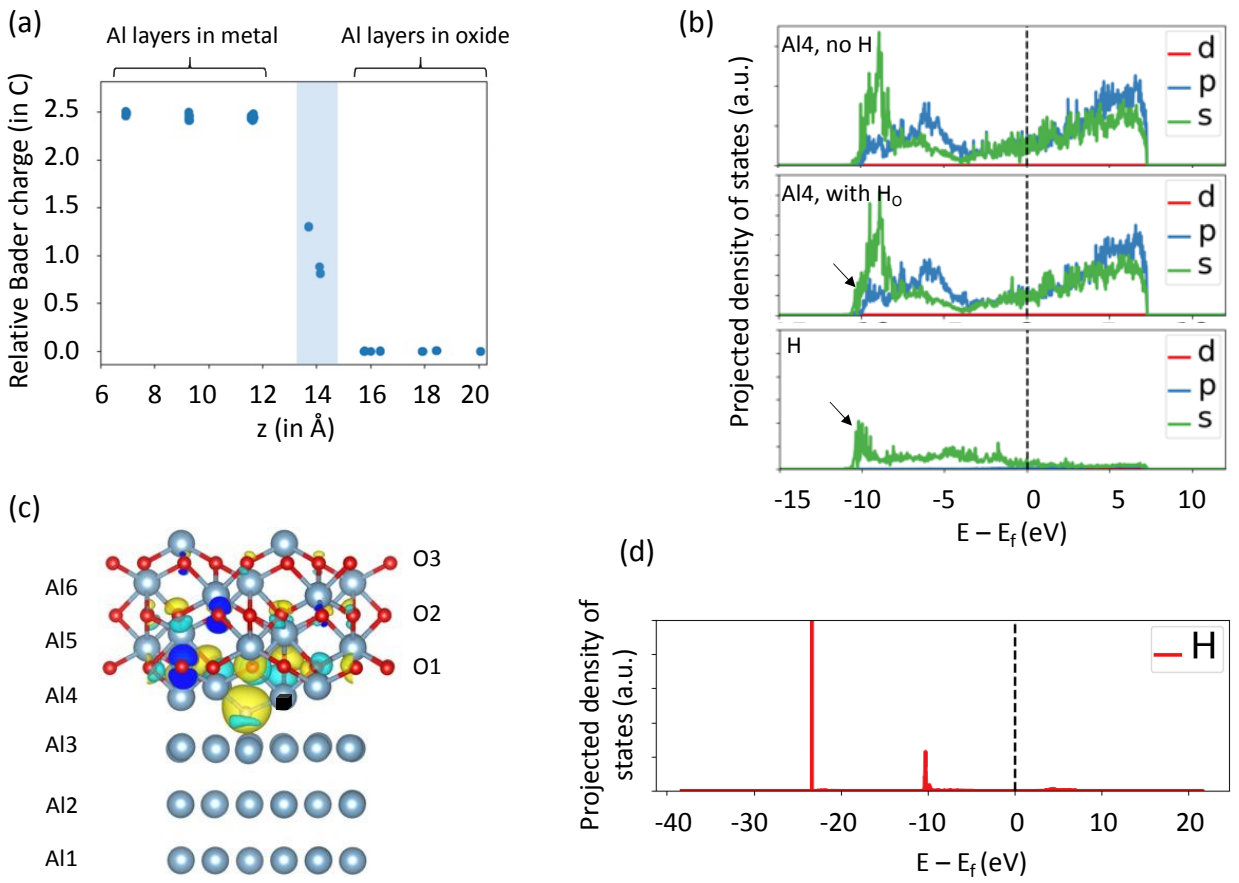


Figure 2. (a) Relative Bader charge (q_{rel}) on Al as a function of its position in the Al|Al_2O_3 simulation cell ($q_{rel} = q_{Al} - q_{Al\ in\ Al2O3\ bulk}$, where q_{Al} is the Bader charge on Al and $q_{Al\ in\ Al2O3\ bulk}$ is the Bader charge on Al in bulk Al_2O_3). (b) From top to bottom: Projected density of states (PDOS) of interfacial Al at oxide side (Al4 Layer) without H defect; PDOS of interfacial Al at oxide side (Al4 Layer) with H_O defect; PDOS of H defect. Overlapping Al and H PDOS are marked with an arrow. Spin-up PDOS is shown, with the Fermi level at 0 eV. (c) Charge density difference (between the interface with H_O and the bare interface) plot, revealing the bonding between under-coordinated Al cations and H. Only the layers near the interface are shown. The oxide layer at the interface has 12.5% V_{Al} as found from ab initio GCMC calculations [21], depicted as a small black cube. (d) Projected density of states (PDOS) of H^+ defect formed upon H donating its electron to mid-gap states and forming an O-H bond, shown by PDOS peak in valence band. Spin-up PDOS is shown. The resulting structure is shown in **Figure 1**e.

While the excess charge accommodated in the interfacial mid-gap states help stabilize H as H^- at the interface, the remaining unoccupied mid-gap states help stabilize H as H^+ in the oxide layer adjacent to the interface, as shown in **Figure 1**e. In contrast to bulk Al_2O_3, where neutral H is a –U center [48,49] and H^+ or H^- will form only in the presence of other acceptor or donor defects (respectively), the presence of empty mid-gap states in the oxide layer adjacent to the interface aid

in the formation and stabilization of H^+ in that layer. From the DOS plot in **Figure 2**d, we see that H prefers to form H^+ and an O-H bond, as seen in the DOS peak deep in the valence band. Thus, the energetic stability from the formation of an O-H bond and the presence of empty mid-gap states near the H defect level results in the formation of H^+ in the oxide layer adjacent to the interface, without requiring the presence of any acceptor defects.

Our second key observation is that the segregation of H to the interface results in the increase in the concentration of aluminum vacancies at the interfacial metal layer through the formation of [V_{Al}-H] complexes. This is explained through **Figure 3**a and 3b, which plot the formation energies of V_{Al}, H, and [V_{Al}-H] defects at the interfacial metal layer and in bulk aluminum, respectively, as a function of hydrogen chemical potential μ_H. Note that by plotting the formation energies over a range of μ_H, our results are agnostic to the particular hydrogen charging mechanism (for example, exposure to hydrogen gas, hydrogen plasma, electrolytic charging with hydrogen, immersion in water, etc.) [50]. Thus, one can calculate the μ_H under different experimental conditions and map it back onto this plot to identify the formation energies and concentrations of different defects.

As μ_H is increased, the formation energy of isolated H defects and [V_{Al}-H] complexes decrease, as expected. However, we also notice that beyond μ_H = -0.03 eV at the interface (**Figure 3**a) and 0.36 eV in bulk metal Al (**Figure 3**b), the formation energy of [V_{Al}-H] is lower than isolated V_{Al}. This indicates that at hydrogen chemical potentials greater than -0.03 eV (for Al|Al_2O_3 system) and 0.36 eV (for bulk Al), hydrogen lowers the formation energy of V_{Al} through the formation of [V_{Al}-H] complexes. This increases the absolute concentration of aluminum vacancies, much higher than the concentrations obtained in the absence of hydrogen, as shown in **Figure 3**c for V_{Al} concentrations at the interfacial metal layer at different temperatures (see Supplementary Information Section S5 [22] for a discussion on how the concentrations were calculated).

This is consistent with the phenomenon called the superabundant vacancy (SAV) formation in bulk metals, which was first experimentally observed in Pd and Ni [51] and later in other metals such as Cu [52], Al [53], Fe [54]. Superabundant vacancy formation occurs when the trapping of hydrogen in the metal vacancy leads to an overall reduction in the energy of formation of the vacancy [55]. This causes the vacancy concentration to increase by several orders of magnitude [55]. DFT analysis has shown that the broken bonds due to under-coordinated metal

atoms around the vacancy are highly reactive and therefore are favorably terminated by H. This gives rise to stabilization of metal vacancies, as well as trapping of H at the vacancy site [55,56].

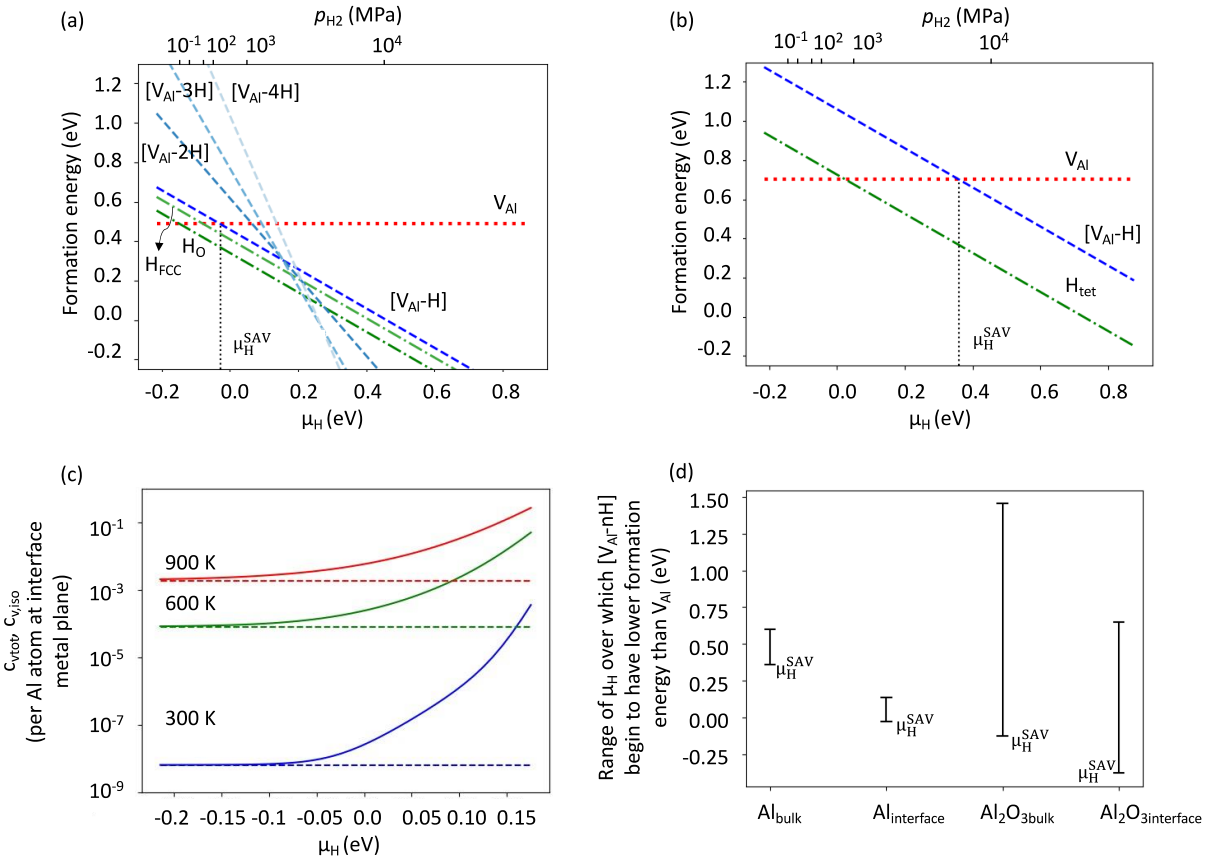


Figure 3. Formation energy of hydrogen and aluminum vacancy (V_{Al}) defects as a function of hydrogen chemical potential, μ_H, (a) at the metal layer of the interface, (b) in bulk Al. μ_H is shown using $\frac{1}{2}\left(\mu_{H_2}^0\right)$ as reference, where $\mu_{H_2}^0$ is the chemical potential of a H_2 molecule at 0 K, i.e., the DFT energy of a H_2 molecule. The corresponding partial pressure of hydrogen gas at 300 K is shown in MPa. Vertical dotted line in (a) and (b) marks the μ_H at which onset of SAV formation occurs (-0.03 and 0.36 eV, at the interface vs. in the metal, respectively). (c) Aluminum vacancy concentration at the interfacial metal layer as a function of hydrogen chemical potential at 300, 600, and 900 K. Dotted lines denote total concentration of isolated aluminum vacancy on interfacial metal plane ($c_{v,iso}$) and solid lines denote total aluminum vacancy concentration (V_{Al} + [V_{Al}-nH]) on interfacial metal plane ($c_{v,tot}$). Note how the total aluminum vacancy concentration begins to increase rapidly at ~-0.03 eV. Note that as long as $\mu_H > \mu_H^{SAV}$, [V_{Al}-nH] complex concentration will be higher than isolated V_{Al} irrespective of the temperature, as the formation energies of the complexes are lower than isolated V_{Al}, as seen in Figure 3a. (d) Summarizing the range of μ_H in bulk Al, at the interfacial metal layer, in bulk Al_2O_3, and at the oxide layer adjacent to the interface, over which [V_{Al}-nH] complexes begin to have lower formation energies than isolated V_{Al}. The lower bound of each range is the μ_H at which onset of SAV formation occurs.

An important difference here is that the onset μ_H for SAV formation at both the metal and oxide sides of the interface is much lower than in bulk Al and in bulk Al_2O_3. As shown in **Figure 3**b and discussed above, SAVs in bulk Al begin to form at μ_H^{SAV} ~ 0.36 eV, i.e., 0.39 eV higher than interfacial μ_H^{SAV}. In fact, μ_H^{SAV} ~ 0.36 eV indicates that formation of SAVs in bulk Al is

unlikely [55], as bulk FCC Al transforms to AlH_3 at ~700 MPa ($\mu_H \sim$ 0.01 eV in **Figure 3**) [57–59] at 300 K. In contrast, μ_H^{SAV} ~ -0.03 eV at the interface indicates that SAVs readily form at the interfacial metal layer, before the transformation of Al to AlH_3. Comparing the shift in μ_H^{SAV} (0.39 eV) with the H-segregation energy (0.39 eV) to the interface, we see that the segregation energy is responsible for the shift in μ_H^{SAV}, thereby lowering the onset μ_H for SAV formation and drastically increasing the [V_{Al}-H] concentration at the interface.

SAV formation can also lead to a rapid increase in H concentration by the trapping of multiple H atoms in the vacancies to form [V_{Al}-nH] complexes (where n is the number of H atoms trapped in V_{Al}) [50,55,60]. Such [V_{Al}-nH] complexes in bulk Al have been investigated in prior studies [50,55] and may have important consequences for hydrogen embrittlement of Al [50,55,60]. We similarly tested the H-trapping effect of V_{Al} at the interfacial metal layer and the formation of [V_{Al}-nH] complexes. The binding energy of hydrogen to V_{Al} (or to an existing [V_{Al}-(n-1)H] complex) at the interfacial metal layer was calculated as

$$E_b([V_{Al} - nH]) = E_f([V_{Al} - (n-1)H]) + E_f(H_O) - E_f([V_{Al} - nH]) \quad (1)$$

i.e., this is the formation energy of an isolated interfacial V_{Al} (or [V_{Al}-(n-1)H] complex) and H_O relative to that of the complex [V_{Al}-nH]. We evaluated the binding energy of a single H atom at different sites and different distances from V_{Al} (shown in Supplementary Information Section S6 [22]), and checked for the possibility of formation of [V_{Al}-nH] complexes by the sequential filling of the sites with favorable (positive) E_b, testing various configurations.

Table 1 (Column 1) shows that it is energetically favorable to trap 4 H atoms in V_{Al} at the interface metal layer, each H occupying either an H_O or the H_{FCC} site. Thus, under high H-loading, non-equilibrium conditions where binding energies play an important role in determining the concentration of defects and their complexes [48,50,61], the positive binding energies in **Table 1** indicate that [V_{Al}-nH] complexes can form. Thus, not only can SAV formation readily occur at the interface, which increases the V_{Al} concentration at the interface metal layer by orders of magnitude; additionally, each resulting V_{Al} from SAV formation can trap multiple H, increasing the effective H concentration at the interface. Together, the rapid increase in V_{Al} and H concentrations can act as precursors to cavitation and blistering of the interface. This enhanced local H concentration may also promote hydride formation at the interface.

Table 1. Binding energies of [V_{Al}-nH] complexes, with V_{Al} at interfacial metal layer (columns 1), V_{Al} at oxide layer adjacent to interface (column 2). Column 3 shows binding energies of Al divacancies and their complexes with hydrogen.

Complex	**E_b (eV)**	**Complex**	**E_b (eV)**	**Complex**	**E_b (eV)**
[V_{Al}-H]	0.37	**[V_{Al}-H]**	2.28	**[V_{Al}-V_{Al}]**	-0.08
[V_{Al}-2H]	0.18	**[V_{Al}-2H]**	1.22	**[[V_{Al}-H]-[V_{Al}-H]**	-0.04
[V_{Al}-3H]	0.18	**[V_{Al}-3H]**	0.44	**[[V_{Al}-2H]-[V_{Al}-2H]]**	0.40
[V_{Al}-4H]	0.07	**[V_{Al}-4H]**	1.63		
		[V_{Al}-5H]	0.70		
		[V_{Al}-6H]	0.02		

We find that hydrogen has similar effects at the oxide layer adjacent to the interface, where it lowers the formation energy for aluminum vacancies by the formation of [V_{Al}-nH] complexes, and can also accumulate at the aluminum vacancies, as shown in Supplementary Information Section S7 [22]. Cation vacancies, such as those in ZrO_2 [62] and Al_2O_3 [12,48] are known to have a strong tendency to accumulate hydrogen. This is because hydrogen prefers to donate its electron to the acceptor states introduced by the cation vacancy (i.e., holes on the oxygen ions surrounding the vacancy), forming O-H bonds [62]. This gives rise to a large binding energy of the cation vacancy-hydrogen defect complex. From Supplementary Figure S5 [22], the defect complex of V_{Al} with one H trapped is the most stable across a wide range of hydrogen chemical potentials and begins to have a lower formation energy than the isolated V_{Al} from μ_H = -0.26 eV. **Figure 1**f shows the structure of this complex, where hydrogen forms O-H bonds with the oxygen atoms at nearest neighbor sites to the V_{Al}. **Table 1** (column 2) tabulates the binding energies of the [V_{Al}-nH] complexes at the oxide layer adjacent to the interface, indicating that a maximum of 5 H can be trapped at the V_{Al} (we do not consider V_{Al}-6H, which as E_b close to room temperature). The binding energy was calculated using Equation 1, replacing $E_f(H_O)$ with $E_f(H_{int})$ (the formation energy of an isolated H at the octahedral interstitial site at the oxide layer adjacent to the interface).

Figure 3d summarizes the discussion above. It plots the range of μ_H over which [V_{Al}-nH] complexes begin to have lower formation energies than isolated V_{Al} in the different systems, comparing the values in bulk to those at the interface. The lower bound of this range is the μ_H at which SAV onset occurs. The upper bound of this range is the maximum μ_H at which a [V_{Al}-nH] defect begins to have lower formation energy than isolated V_{Al}. The formation energy vs. μ_H plot for [V_{Al}-nH] complexes in bulk Al_2O_3 (from which the μ_H range shown in **Figure 3**d was

extracted) is given in Supplementary Information Section S8 [22]. At the interface and at the oxide layer adjacent to the interface, the onset μ_H for SAVs are lower than their counterparts in bulk Al and Al_2O_3; additionally, [V_{Al}-nH] complexes become more stable than V_{Al} at lower μ_H compared to their counterparts in bulk Al and Al_2O_3. Note that the range for Al_{bulk} was taken from Nazarov et al. [55]

Finally, we also investigated aluminum divacancies at the interfacial metal layer. Divacancies are known to be unstable in bulk Al [60,63] but can be stabilized by the trapping of multiple H in each vacancy [60]. From the binding energies reported in **Table 1** (Column 3), similar to that in the Al bulk, Al divacancies are unstable at the interface. However, we find that trapping of 2 H in each vacancy can stabilize a divacancy at the interface. Thus, divacancies can favorably form at the hydrogenated interface, accelerating damage and acting as precursors to the formation of cavities and microvoids [11,14,60].

We now discuss the implications of this understanding of hydrogen behavior at the Al|Al_2O_3 interface. We begin by noting that although the activation energy (E_a) for hydrogen diffusion in Al_2O_3 is very high (E_a ~ 2.25 eV in single crystal Al_2O_3 [64]), hydrogen can still reach the interface via fast diffusion pathways such as dislocations, grain boundaries, or cracks in the Al_2O_3 layer (E_a in polycrystalline Al_2O_3 is ~1.89 eV [64]). Hydrogen can also reach the interface from the Al layer (E_a ~0.46 eV in single crystal Al [65]). Ultimately, given that experiments (as discussed below and in the Introduction) report interfacial damage due to hydrogen present at the interface, our study provides insight into the potential causes behind this damage once the hydrogen reaches the interface.

In the context of coatings and passive oxide layers, the low formation energies of H_O and H_{FCC} at the interface indicate that when (if) hydrogen diffuses through Al_2O_3 passivation layer and reaches the interface, it will remain trapped at the interface, and slow down hydrogen diffusion across this interface. This indicates that multilayer coatings with alternating layers of Al_2O_3 and Al could provide high hydrogen permeation resistance by trapping hydrogen at the interfaces. Some studies have alluded to this [66]. We also gain insight into the atomistic mechanisms that could initiate cavitation and blistering at the interface. Comparing the energetics of the different defects in the metal versus oxide sides of the interface, we see that the V_{Al} and [V_{Al}-nH] defect formation energetics at the Al metal side are much more favorable. Thus, damage most likely initiates at the

Al side, due to H accumulation at the interface, SAV formation, and [V_{Al}-nH] complex formation at the interfacial Al metal layer. The increased V_{Al} concentration due to SAV formation can weaken the interface and facilitate metal diffusion required for cavity formation and growth observed in experiments [11,14]. The increased hydrogen concentration can ultimately form hydrogen molecules, leading to bubbles and blistering, or even the formation of a hydride phase.

In the context of electronic devices, the increase in electronic conductivity observed upon hydration of Al|Al_2O_3|Al tunnel junctions could be due to the empty mid-gap states at the oxide layer adjacent to the interface accepting electrons from H to stabilize H^+. Thus, the mechanism of H as an n-type dopant must be considered in conjunction with the increase in electronic conductivity due to tunneling via H defects as mentioned in prior work [15]. Our study also helps identify which hydrogen defects could be the predominant sources for decoherence in superconducting qubits. From our hydrogen defect formation energies explicitly at different regions near the interface, we find that in the oxide layer adjacent to the interface, [V_{Al}-H] has the least formation energy across the entire range of hydrogen chemical potential, and therefore has the highest concentration. Thus, it could be an important source of decoherence, as reported for bulk Al_2O_3 [19], along with H^+ in the octahedral interstitial site [20].

Acknowledgements

We thank Dr. Konstantin Klyukin and Dr. Pjotrs Žguns for helpful discussions. This work has been supported by the U.S. Department of Energy, Office of Science, Office of Energy Efficiency & Renewable Energy, under Award number DE-EE0008830. This work used the Extreme Science and Engineering Discovery Environment (XSEDE) resources [67] Stampede2 at the Texas Advanced Computing Center (TACC) and Expanse at the San Diego Supercomputer Center (SDSC) through allocation number TG-DMR120025. XSEDE is supported by National Science Foundation grant number ACI-1548562. This work also used Frontera [68] at the Texas Advanced Computing Center through allocation number DMR20012. We thank the staff at TACC and SDSC for technical support.

Author contributions

V.S. performed the simulations. B.Y. supervised the work. Both authors discussed the results and wrote the manuscript.

References

[1] Z. Yin, S. Tao, X. Zhou, and C. Ding, *Microstructure and Mechanical Properties of Al2O3–Al Composite Coatings Deposited by Plasma Spraying*, Applied Surface Science **254**, 1636 (2008).

[2] Y. Xin, C. Liu, W. Zhang, J. Jiang, G. Tang, X. Tian, and P. K. Chu, *Electrochemical Behavior Al2O3 / Al Coated Surgical AZ91 Magnesium Alloy in Simulated Body Fluids*, J. Electrochem. Soc. **155**, C178 (2008).

[3] W. Zhang and J. R. Smith, *Nonstoichiometric Interfaces and Al2O3 Adhesion with Al and Ag*, Phys. Rev. Lett. **85**, 3225 (2000).

[4] J. D. Baran, H. Grönbeck, and A. Hellman, *Mechanism for Limiting Thickness of Thin Oxide Films on Aluminum*, Phys. Rev. Lett. **112**, 146103 (2014).

[5] N. P. de Leon, K. M. Itoh, D. Kim, K. K. Mehta, T. E. Northup, H. Paik, B. S. Palmer, N. Samarth, S. Sangtawesin, and D. W. Steuerman, *Materials Challenges and Opportunities for Quantum Computing Hardware*, Science **372**, eabb2823 (2021).

[6] R. Winter, I. Krylov, C. Cytermann, K. Tang, J. Ahn, P. C. McIntyre, and M. Eizenberg, *Fermi Level Pinning in Metal/Al2O3/InGaAs Gate Stack after Post Metallization Annealing*, Journal of Applied Physics **118**, 055302 (2015).

[7] S. Oh, K. Cicak, J. S. Kline, M. A. Sillanpää, K. D. Osborn, J. D. Whittaker, R. W. Simmonds, and D. P. Pappas, *Elimination of Two Level Fluctuators in Superconducting Quantum Bits by an Epitaxial Tunnel Barrier*, Phys. Rev. B **74**, 100502 (2006).

[8] L. Jiang, Z. Li, G. Fan, and D. Zhang, *A Flake Powder Metallurgy Approach to Al2O3/Al Biomimetic Nanolaminated Composites with Enhanced Ductility*, Scripta Materialia **65**, 412 (2011).

[9] N. Burgos, M. Paulis, M. Mirari Antxustegi, and M. Montes, *Deep Oxidation of VOC Mixtures with Platinum Supported on Al2O3/Al Monoliths*, Applied Catalysis B: Environmental **38**, 251 (2002).

[10] A. V. Parmuzina and O. V. Kravchenko, *Activation of Aluminium Metal to Evolve Hydrogen from Water*, International Journal of Hydrogen Energy **33**, 3073 (2008).

[11] D.-G. Xie, Z.-J. Wang, J. Sun, J. Li, E. Ma, and Z.-W. Shan, *In Situ Study of the Initiation of Hydrogen Bubbles at the Aluminium Metal/Oxide Interface*, Nature Mater **14**, 9 (2015).

[12] S. N. Rashkeev, K. W. Sohlberg, S. Zhuo, and S. T. Pantelides, *Hydrogen-Induced Initiation of Corrosion in Aluminum*, J. Phys. Chem. C **111**, 7175 (2007).

[13] Y. Liu, M. Alexander, E. Koroleva, P. Skeldon, G. E. Thompson, P. Bailey, T. C. Q. Noakes, K. Shimizu, and H. Habazaki, *Detachment of Alumina Films from Aluminium by 100 KeV H+ Ions*, Surface and Interface Analysis **33**, 318 (2002).

[14] M. Li, D.-G. Xie, E. Ma, J. Li, X.-X. Zhang, and Z.-W. Shan, *Effect of Hydrogen on the Integrity of Aluminium–Oxide Interface at Elevated Temperatures*, Nat Commun **8**, 1 (2017).

[15] D. R. Jennison, P. A. Schultz, and J. P. Sullivan, *Evidence for Interstitial Hydrogen as the Dominant Electronic Defect in Nanometer Alumina Films*, Phys. Rev. B **69**, 041405 (2004).

[16] A. C. Kozen, M. A. Schroeder, K. D. Osborn, C. J. Lobb, and G. W. Rubloff, *Examining the Role of Hydrogen in the Electrical Performance of in Situ Fabricated Metal-Insulator-Metal Trilayers Using an Atomic Layer Deposited Al2O3 Dielectric*, Appl. Phys. Lett. **102**, 173501 (2013).

[17] J. C. Barbour, R. G. Copeland, R. G. Dunn, N. Missert, L. P. Montes, K.-A. Son, and J. P. Sullivan, The Electrical Properties of Native and Deposited Thin Aluminum Oxide Layers on Aluminum: Hydration Effects, No. SAND98-2534C, Sandia National Laboratories (SNL), Albuquerque, NM, and Livermore, CA (United States), 1998.
[18] M. S. Khalil, M. J. A. Stoutimore, S. Gladchenko, A. M. Holder, C. B. Musgrave, A. C. Kozen, G. Rubloff, Y. Q. Liu, R. G. Gordon, J. H. Yum et al., *Evidence for Hydrogen Two-Level Systems in Atomic Layer Deposition Oxides*, Appl. Phys. Lett. **103**, 162601 (2013).
[19] A. M. Holder, K. D. Osborn, C. J. Lobb, and C. B. Musgrave, *Bulk and Surface Tunneling Hydrogen Defects in Alumina*, Phys. Rev. Lett. **111**, 065901 (2013).
[20] L. Gordon, H. Abu-Farsakh, A. Janotti, and C. G. Van de Walle, *Hydrogen Bonds in Al2O3 as Dissipative Two-Level Systems in Superconducting Qubits*, Sci Rep **4**, 1 (2014).
[21] V. Somjit and B. Yildiz, *Atomic and Electronic Structure of the Al2O3/Al Interface during Oxide Propagation Probed by Ab Initio Grand Canonical Monte Carlo*, ACS Appl. Mater. Interfaces **14**, 42613 (2022).
[22] See Supplemental Material at [URL Will Be Inserted by Publisher] for Additional Details on Simulation Methodology., (n.d.).
[23] J. Kang, J. Zhu, C. Curtis, D. Blake, G. Glatzmaier, Y.-H. Kim, and S.-H. Wei, *Atomically Abrupt Liquid-Oxide Interface Stabilized by Self-Regulated Interfacial Defects: The Case of Al/Al2O3 Interfaces*, Phys. Rev. Lett. **108**, 226105 (2012).
[24] L. P. H. Jeurgens, W. G. Sloof, F. D. Tichelaar, and E. J. Mittemeijer, *Structure and Morphology of Aluminium-Oxide Films Formed by Thermal Oxidation of Aluminium*, Thin Solid Films **418**, 89 (2002).
[25] D. L. Medlin, K. F. McCarty, R. Q. Hwang, S. E. Guthrie, and M. I. Baskes, *Orientation Relationships in Heteroepitaxial Aluminum Films on Sapphire*, Thin Solid Films **299**, 110 (1997).
[26] Z. Cheng, Y. R. Koh, H. Ahmad, R. Hu, J. Shi, M. E. Liao, Y. Wang, T. Bai, R. Li, E. Lee et al., *Thermal Conductance across Harmonic-Matched Epitaxial Al-Sapphire Heterointerfaces*, Commun Phys **3**, 1 (2020).
[27] G. Pilania, B. J. Thijsse, R. G. Hoagland, I. Lazić, S. M. Valone, and X.-Y. Liu, *Revisiting the Al/Al2O3 Interface: Coherent Interfaces and Misfit Accommodation*, Sci Rep **4**, 1 (2014).
[28] D. Ma, Z. Lu, Y. Tang, T. Li, Z. Tang, and Z. Yang, *Effect of Lattice Strain on the Oxygen Vacancy Formation and Hydrogen Adsorption at CeO2(111) Surface*, Physics Letters A **378**, 2570 (2014).
[29] D. J. Siegel, L. G. Hector, and J. B. Adams, *Adhesion, Atomic Structure, and Bonding at the Al(111)/Al2O3(0001) Interface: A First Principles Study*, Phys. Rev. B **65**, 085415 (2002).
[30] G. Kresse and J. Hafner, *Ab Initio Molecular-Dynamics Simulation of the Liquid-Metal--Amorphous-Semiconductor Transition in Germanium*, Phys. Rev. B **49**, 14251 (1994).
[31] G. Kresse and J. Hafner, *Ab Initio Molecular Dynamics for Liquid Metals*, Phys. Rev. B **47**, 558 (1993).
[32] G. Kresse and J. Furthmüller, *Efficiency of Ab-Initio Total Energy Calculations for Metals and Semiconductors Using a Plane-Wave Basis Set*, Computational Materials Science **6**, 15 (1996).
[33] G. Kresse and J. Furthmüller, *Efficient Iterative Schemes for Ab Initio Total-Energy Calculations Using a Plane-Wave Basis Set*, Phys. Rev. B **54**, 11169 (1996).

[34] G. Kresse and D. Joubert, *From Ultrasoft Pseudopotentials to the Projector Augmented-Wave Method*, Phys. Rev. B **59**, 1758 (1999).
[35] P. E. Blöchl, *Projector Augmented-Wave Method*, Phys. Rev. B **50**, 17953 (1994).
[36] J. P. Perdew, K. Burke, and M. Ernzerhof, *Generalized Gradient Approximation Made Simple*, Phys. Rev. Lett. **77**, 3865 (1996).
[37] S. B. Zhang and J. E. Northrup, *Chemical Potential Dependence of Defect Formation Energies in GaAs: Application to Ga Self-Diffusion*, Phys. Rev. Lett. **67**, 2339 (1991).
[38] C. G. Van de Walle, D. B. Laks, G. F. Neumark, and S. T. Pantelides, *First-Principles Calculations of Solubilities and Doping Limits: Li, Na, and N in ZnSe*, Phys. Rev. B **47**, 9425 (1993).
[39] H. Wipf, *Solubility and Diffusion of Hydrogen in Pure Metals and Alloys*, Phys. Scr. **2001**, 43 (2001).
[40] Y. Fukai, *Metal-Hydrogen System Under Extended p, T Conditions*, in *The Metal-Hydrogen System: Basic Bulk Properties*, edited by Y. Fukai (Springer, Berlin, Heidelberg, 1993), pp. 71–119.
[41] H. Sugimoto and Y. Fukai, *Solubility of Hydrogen in Metals under High Hydrogen Pressures: Thermodynamical Calculations*, Acta Metallurgica et Materialia **40**, 2327 (1992).
[42] C. Wolverton, V. Ozoliņš, and M. Asta, *Hydrogen in Aluminum: First-Principles Calculations of Structure and Thermodynamics*, Phys. Rev. B **69**, 144109 (2004).
[43] C. Freysoldt, B. Grabowski, T. Hickel, J. Neugebauer, G. Kresse, A. Janotti, and C. G. Van de Walle, *First-Principles Calculations for Point Defects in Solids*, Rev. Mod. Phys. **86**, 253 (2014).
[44] W. Tang, E. Sanville, and G. Henkelman, *A Grid-Based Bader Analysis Algorithm without Lattice Bias*, J. Phys.: Condens. Matter **21**, 084204 (2009).
[45] E. Sanville, S. D. Kenny, R. Smith, and G. Henkelman, *Improved grid-based algorithm for Bader charge allocation*, Journal of Computational Chemistry **28**, 899 (2007).
[46] S. Zhao, E. Kan, and Z. Li, *Electride: From Computational Characterization to Theoretical Design*, WIREs Computational Molecular Science **6**, 430 (2016).
[47] A. Janotti and C. G. Van de Walle, *Hydrogen Multicentre Bonds*, Nature Mater **6**, 1 (2007).
[48] V. Somjit and B. Yildiz, *Doping α-Al2O3 to Reduce Its Hydrogen Permeability: Thermodynamic Assessment of Hydrogen Defects and Solubility from First Principles*, Acta Materialia **169**, 172 (2019).
[49] G. Zhang, Y. Lu, and X. Wang, *Hydrogen Interactions with Intrinsic Point Defects in Hydrogen Permeation Barrier of α-Al2O3 : A First-Principles Study*, Physical Chemistry Chemical Physics **16**, 17523 (2014).
[50] L. Ismer, M. S. Park, A. Janotti, and C. G. Van de Walle, *Interactions between Hydrogen Impurities and Vacancies in Mg and Al: A Comparative Analysis Based on Density Functional Theory*, Phys. Rev. B **80**, 184110 (2009).
[51] Y. F. Y. Fukai and N. Ō. N. Ōkuma, *Evidence of Copious Vacancy Formation in Ni and Pd under a High Hydrogen Pressure*, Jpn. J. Appl. Phys. **32**, L1256 (1993).
[52] Y. Fukai, M. Mizutani, S. Yokota, M. Kanazawa, Y. Miura, and T. Watanabe, *Superabundant Vacancy–Hydrogen Clusters in Electrodeposited Ni and Cu*, Journal of Alloys and Compounds **356–357**, 270 (2003).
[53] H. K. Birnbaum, C. Buckley, F. Zeides, E. Sirois, P. Rozenak, S. Spooner, and J. S. Lin, *Hydrogen in Aluminum*, Journal of Alloys and Compounds **253–254**, 260 (1997).

[54] Y. Fukai, T. Haraguchi, E. Hayashi, Y. Ishii, Y. Kurokawa, and J. Yanagawa, *Hydrogen-Induced Superabundant Vacancies and Diffusion Enhancement in Some FCC Metals*, Defect and Diffusion Forum **194–199**, 1063 (2001).
[55] R. Nazarov, T. Hickel, and J. Neugebauer, *Ab Initio Study of H-Vacancy Interactions in Fcc Metals: Implications for the Formation of Superabundant Vacancies*, Phys. Rev. B **89**, 144108 (2014).
[56] Y. Tateyama and T. Ohno, *Stability and Clusterization of Hydrogen-Vacancy Complexes in α-Fe: An Ab Initio Study*, Phys. Rev. B **67**, 174105 (2003).
[57] H. Saitoh, A. Machida, Y. Katayama, and K. Aoki, *Formation and Decomposition of AlH3 in the Aluminum-Hydrogen System*, Appl. Phys. Lett. **93**, 151918 (2008).
[58] B. Baranowski and M. Tkacz, *The Equilibrium Between Solid Aluminium Hydride and Gaseous Hydrogen*, Zeitschrift Für Physikalische Chemie **135**, 27 (1983).
[59] G. C. Sinke, L. C. Walker, F. L. Oetting, and D. R. Stull, *Thermodynamic Properties of Aluminum Hydride*, J. Chem. Phys. **47**, 2759 (1967).
[60] G. Lu and E. Kaxiras, *Hydrogen Embrittlement of Aluminum: The Crucial Role of Vacancies*, Phys. Rev. Lett. **94**, 155501 (2005).
[61] C. G. Van de Walle and J. Neugebauer, *First-Principles Calculations for Defects and Impurities: Applications to III-Nitrides*, Journal of Applied Physics **95**, 3851 (2004).
[62] M. Youssef and B. Yildiz, *Hydrogen Defects in Tetragonal ZrO 2 Studied Using Density Functional Theory*, Physical Chemistry Chemical Physics **16**, 1354 (2014).
[63] K. Carling, G. Wahnström, T. R. Mattsson, A. E. Mattsson, N. Sandberg, and G. Grimvall, *Vacancies in Metals: From First-Principles Calculations to Experimental Data*, Phys. Rev. Lett. **85**, 3862 (2000).
[64] J. D. Fowler, D. Chandra, T. S. Elleman, A. W. Payne, and K. Verghese, *Tritium Diffusion in A12O3 and BeO*, Journal of the American Ceramic Society **60**, 155 (1977).
[65] M. Ichimura, Y. Sasajima, and M. Imabayashi, *Grain Boundary Effect on Diffusion of Hydrogen in Pure Aluminum*, Materials Transactions, JIM **32**, 1109 (1991).
[66] J. Yamabe, S. Matsuoka, and Y. Murakami, *Surface Coating with a High Resistance to Hydrogen Entry under High-Pressure Hydrogen-Gas Environment*, International Journal of Hydrogen Energy **38**, 10141 (2013).
[67] J. Towns, T. Cockerill, M. Dahan, I. Foster, K. Gaither, A. Grimshaw, V. Hazlewood, S. Lathrop, D. Lifka, G.D. Peterson et al., *XSEDE: Accelerating Scientific Discovery*, Computing in Science & Engineering **16**, 62 (2014).
[68] D. Stanzione, J. West, R. T. Evans, T. Minyard, O. Ghattas, and D. K. Panda, *Frontera: The Evolution of Leadership Computing at the National Science Foundation*, in *Practice and Experience in Advanced Research Computing* (Association for Computing Machinery, New York, NY, USA, 2020), pp. 106–111.